Supplemental Information

Crystal structures of an unmodified bacterial tRNA reveal intrinsic structural flexibility and plasticity as general properties of unbound tRNAs

Clarence W Chan[1], Deanna Badong[1], Rakhi Rajan[1,2] and Alfonso Mondragón[1,3]

[1] Department of Molecular Biosciences, Northwestern University, 2205 Tech Drive, Evanston, IL 60208-3500

[2] Present address: Department of Chemistry and Biochemistry, Price Family Foundation Institute of Structural Biology, Stephenson Life Sciences Research Center, University of Oklahoma, 101 Stephenson Parkway, Norman, OK 73019-5251

[3] To whom correspondence should be addressed. Tel: +1-847-491-7726; Fax: +1-847-467-6489; Email: a-mondragon@northwestern.edu

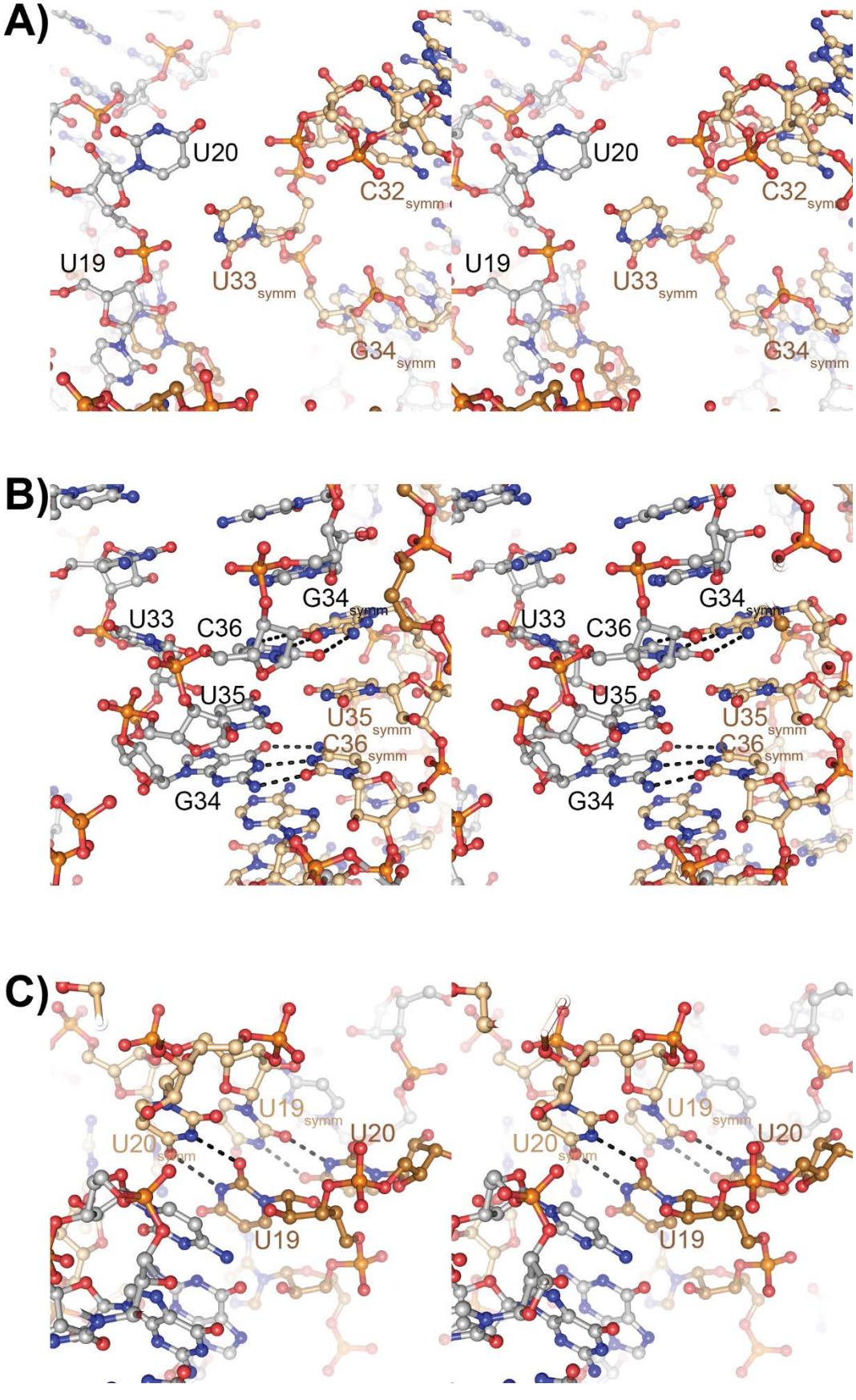
A)
U20
C32 symm
U19
U33 symm
G34 symm
U20
C32 symm
U19
U33 symm
G34 symm
B)
U33
C36
G34 symm
U35
U35 symm
C36 symm
G34
U33
C36
G34 symm
U35
U35 symm
C36 symm
G34
C)
U19 symm
U20
U20 symm
U19
U19 symm
U20
U20 symm
U19

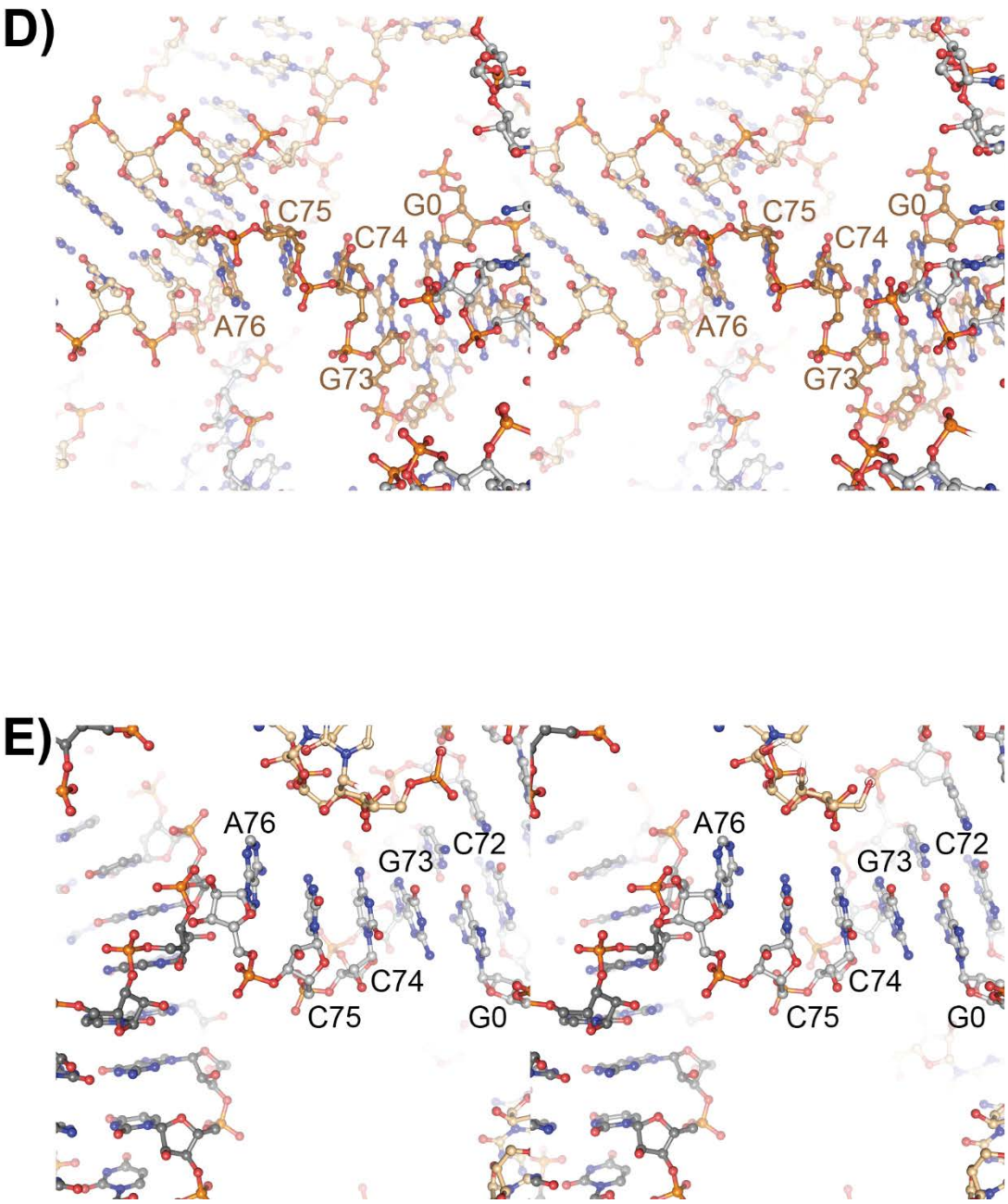

Supplementary Figure S1. Crystallographic lattice contacts are not responsible for most of the structural changes observed between the two monomers making up the *Escherichia coli* tRNA^{Asp} crystal. A) Stereo diagram showing the contacts between U20 in the A monomer (grey) and U33 in a symmetry related B monomer (tan). The two nucleotides face each other but do not make direct contacts. **B)** Stereo diagram showing the contacts between the anticodon

triplet (G34, U35, and C36) of an A monomer (grey) with the equivalent region in a B monomer (tan). Note that U33 in the A monomer faces C36, whereas U33 in the B monomer (panel **A**) faces the solvent. This conformational difference cannot be attributed to lattice contacts. **C)** Stereo diagram showing the contacts between U19 and U20 of a B monomer (tan) with the equivalent nucleotides in a symmetry related B monomer (brown). **D)** Stereo diagram showing the contacts between the CCA tail at the 3' end of the B monomer (brown) and surrounding molecules. **E)** Stereo diagram showing the contacts between the CCA tail at the 3' end of the B monomer (grey) and surrounding molecules. Note that the 3' end of the two monomers adopt different conformations and make different lattice contacts probably as this region is unpaired and more mobile.

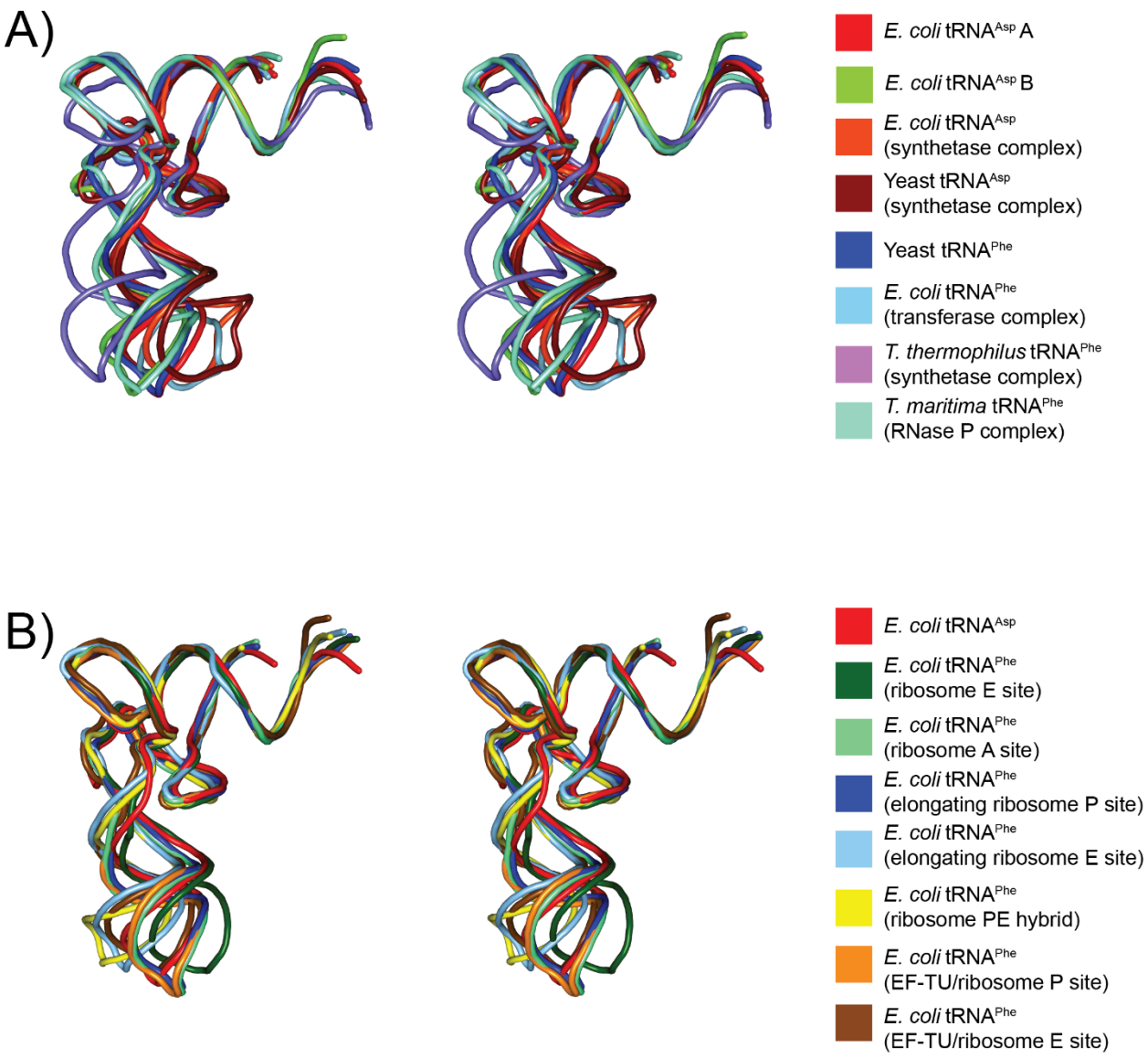

Supplementary Figure S2. Overall structural comparison between *E. coli* tRNA^{Asp} and tRNAs from different complexes. A) Alignments and comparison between tRNAs found in complex with aminoacyl tRNA synthetases, isopentenyl-tRNA transferase, and bacterial RNase P. Red: *E. coli* tRNA^{Asp} A monomer. Green: *E. coli* tRNA^{Asp} B monomer. Orange: *E. coli* tRNA^{Asp} from a complex with *Thermus thermophilus* aspartyl-tRNA synthetase (PDB ID: 1EFW) (Briand et al. 2000). Brown: *Saccharomyces cerevisiae* tRNA^{Asp} from a complex with *S. cerevisiae* aspartyl-tRNA synthetase (PDB ID: 1ASY) (Ruff et al. 1991). Blue: *S. cerevisiae* tRNA^{Phe} (PDB

ID 1EHZ) (Shi and Moore 2000). Light blue: *E. coli* $tRNA^{Phe}$ from a complex with *E. coli* isopentyl-tRNA transferase (PDB ID 3FOZ) (Seif and Hallberg 2009). Purple: *T. thermophilus* $tRNA^{Phe}$ from a complex with *T. thermophilus* phenylanalyl-tRNA synthetase (PDB ID: 1EIY) (Goldgur et al. 1997). Aquamarine: *Thermatoga maritima* $tRNA^{Phe}$ from a complex with *T. maritima* RNase P (PDB ID: 3Q1Q) (Reiter et al. 2010). **B)** Alignments and comparison between tRNAs found within ribosome structures. Red: *E. coli* $tRNA^{Asp}$. Dark green: *E. coli* $tRNA^{Phe}$ in the E site of the *T. thermophilus* ribosome (PDB ID: 4V5D) (Voorhees et al. 2009). Light green: Charged *E. coli* $tRNA^{Phe}$ in the A site of the *T. thermophilus* ribosome (PDB ID: 4V5D) (Voorhees et al. 2009). Dark blue: *E. coli* $tRNA^{Phe}$ in the P site in the elongating *T. thermophilus* ribosome (PDB ID: 4V6F) (Jenner et al. 2010). Light blue: *E. coli* $tRNA^{Phe}$ in the E site in the elongating *T. thermophilus* ribosome (PDB ID: 4V6F) (Jenner et al. 2010). Yellow: *E. coli* $tRNA^{Phe}$ in a PE hybrid state in the *T. thermophilus* ribosome (PDB ID: 4V9H) (Tourigny et al. 2013). Orange: *E. coli* $tRNA^{Phe}$ in the P site of the *T. thermophilus* ribosome in complex with EF-TU and aminoacyl-tRNA (PDB ID: 4V5G) (Schmeing et al. 2009). Brown: *E. coli* $tRNA^{Phe}$ in the E site of the *T. thermophilus* ribosome in complex with EF-TU and aminoacyl-tRNA (PDB ID: 4V5G) (Schmeing et al. 2009). For the alignments, the acceptor stems of the different tRNAs were superposed using *E. coli* $tRNA^{Asp}$ as a reference.

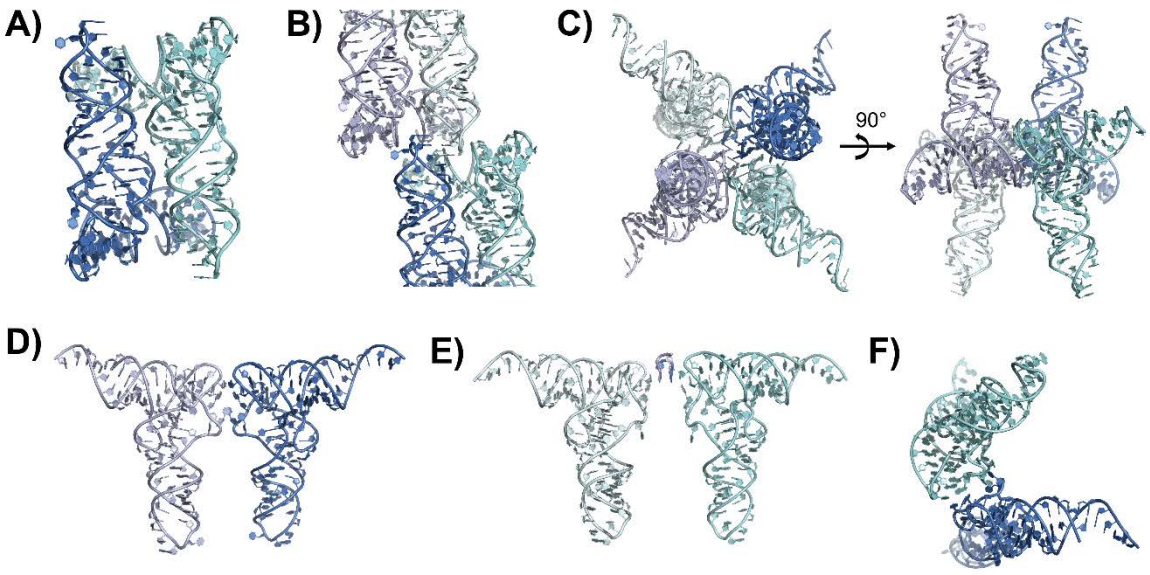

Supplementary Figure S3. Crystallographic lattice contacts made by *E. coli* tRNA^{Asp}. Relatively few crystallographic lattice contacts enable the crystallization of *E. coli* tRNA^{Asp} and they encompass the frequently occurring coaxial-stacking (**A**), base pairing (**B**), and base stacking interactions (same region shown in multiple orientations in **C** – **F**).

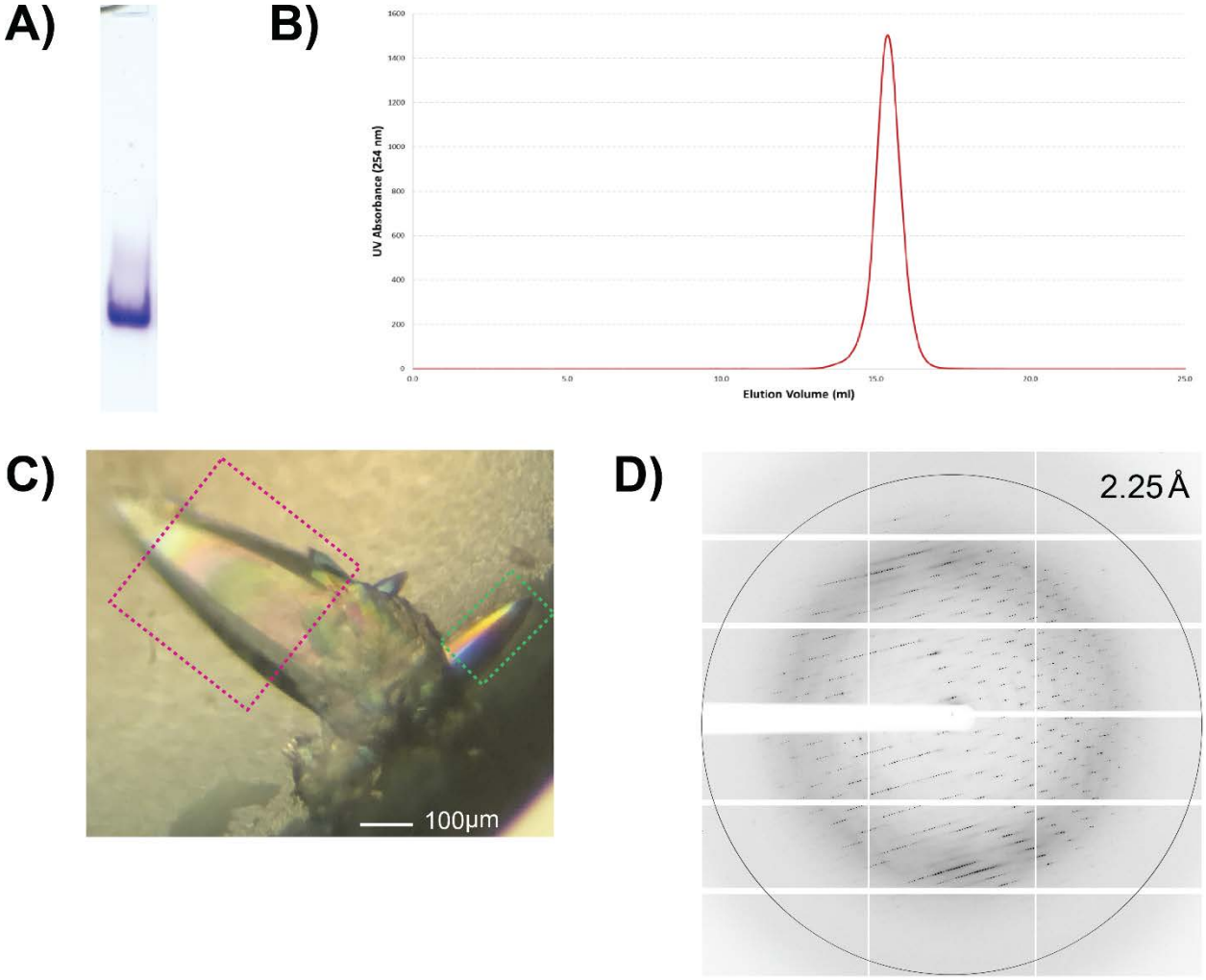

Supplementary Figure S4. Purification, crystallization, and X-ray diffraction data collection of *E. coli* tRNA^{Asp}. A) *In vitro* transcribed *E. coli* tRNA^{Asp} was purified to apparent homogeneity, as assessed by a 10% (v/v) polyacrylamide native gel stained with Toluidine Blue-O. **B)** Size-exclusion chromatography demonstrated that purified *E. coli* tRNA^{Asp} is monodispersed in solution. **C)** Crystals of *E. coli* tRNA^{Asp} tended to grow in clusters. Manual manipulation was needed to excise fragments suitable for data collection (for example, pink and green dotted boxes). **D)** X-ray diffraction limit of *E. coli* tRNA^{Asp} crystals was approximately 2 Å (~2.4 Å diffraction data shown).

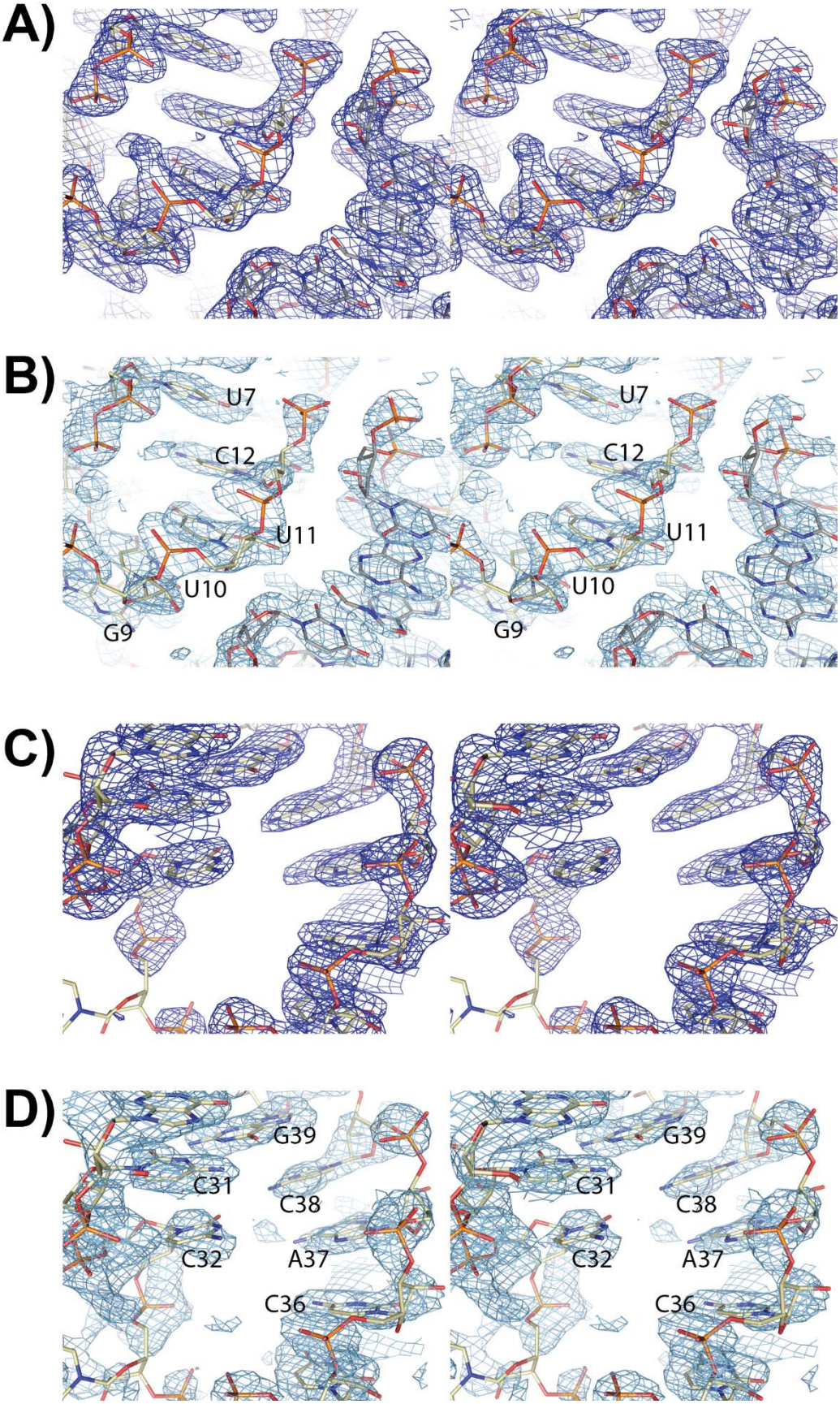
A)
B)
U7
C12
U11
U10
G9
U7
C12
U11
U10
G9
C)
D)
G39
C31
C38
C32
A37
C36
G39
C31
C38
C32
A37
C36

Supplementary Figure S5. Electron density maps of the *E. coli* tRNA^{Asp} structure. Stereo diagrams showing **2mF$_O$-DF$_C$** (**A** and **C**) and simulated annealing omit maps (**B** and **D**) around different regions of the structure. The maps in panels **A** and **B** and in **C** and **D** correspond to the same region in the structure.

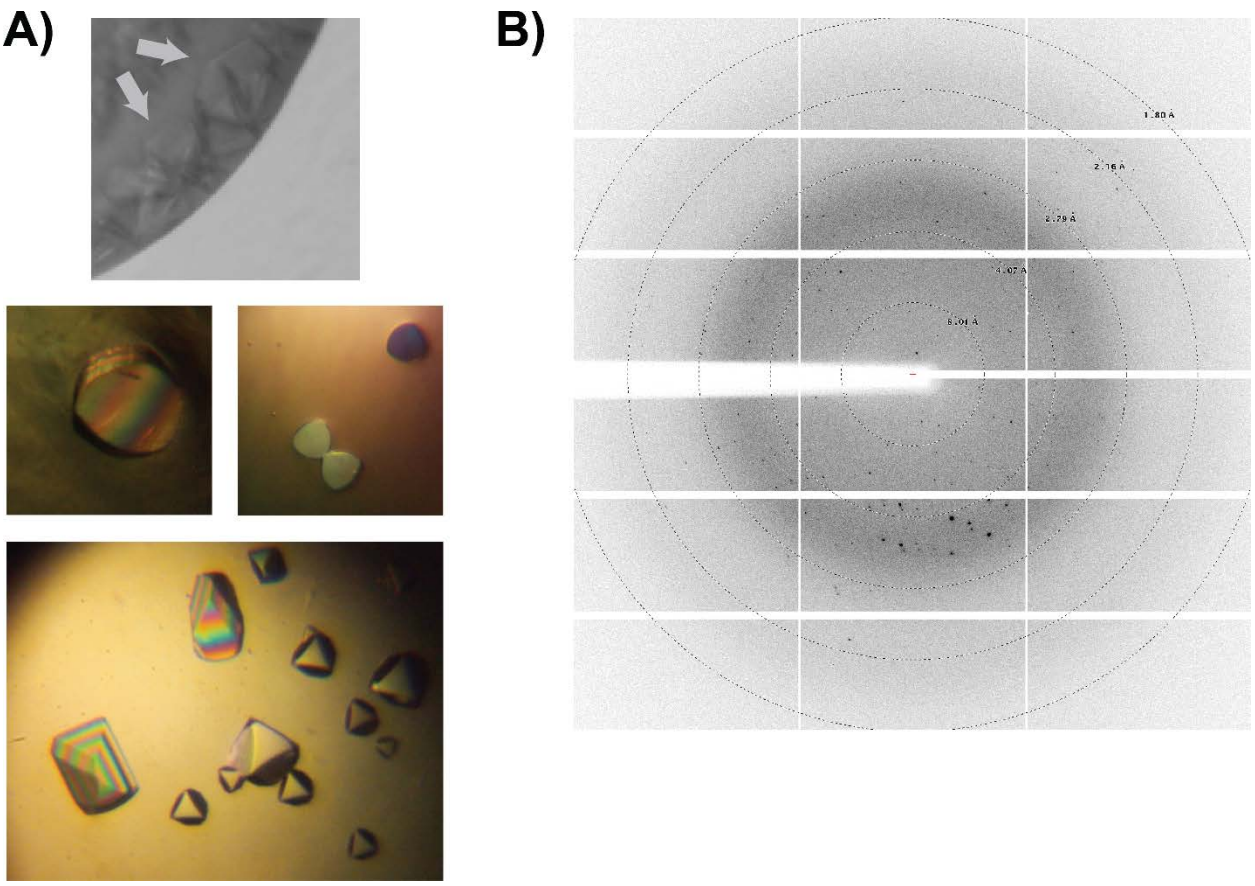

Supplementary Figure S6. Crystallization and X-ray diffraction data collection of *E. coli* tRNA^{Asp}-AS/TSL. A) Crystals of *E. coli* tRNA^{Asp}-AS/TSL (arrows). **B)** X-ray diffraction limit of *E. coli* tRNA^{Asp} crystals was between 1.6 – 1.7 Å with high anisotropy.

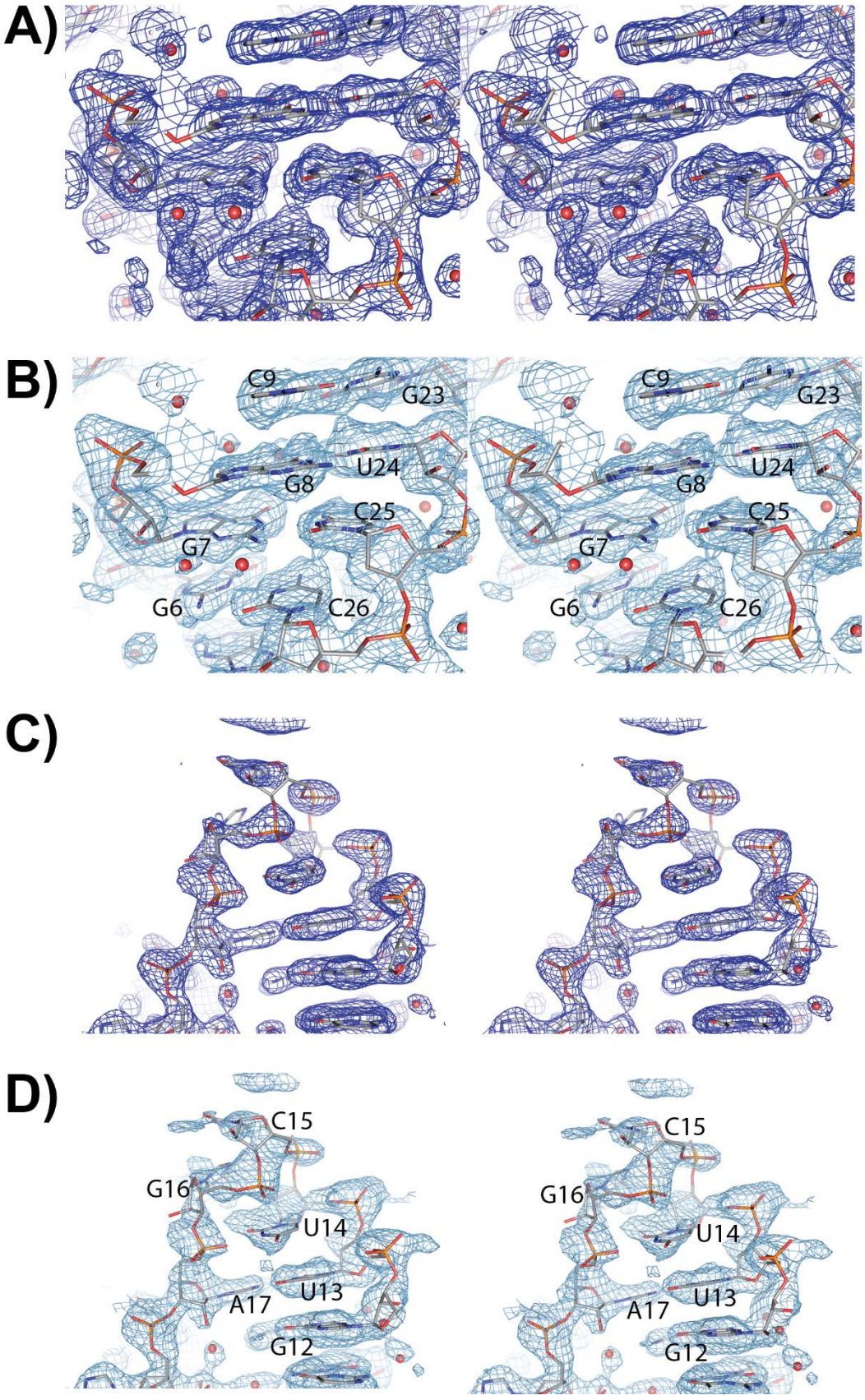
A)
B)
C9
G23
U24
G8
C25
G7
G6
C26
C)
D)
C15
G16
U14
A17
U13
G12

Supplementary Figure S7. Electron density maps of the *E. coli* tRNA^{Asp}-AS/TSL long unit cell structure. Stereo diagrams showing **2mF$_o$-DF$_c$** (**A** and **C**) and simulated annealing omit maps (**B** and **D**) around different regions of the structure. The maps in panels **A** and **B** show a well-ordered region in the stem, whereas panels **C** and **D** show the loop region.

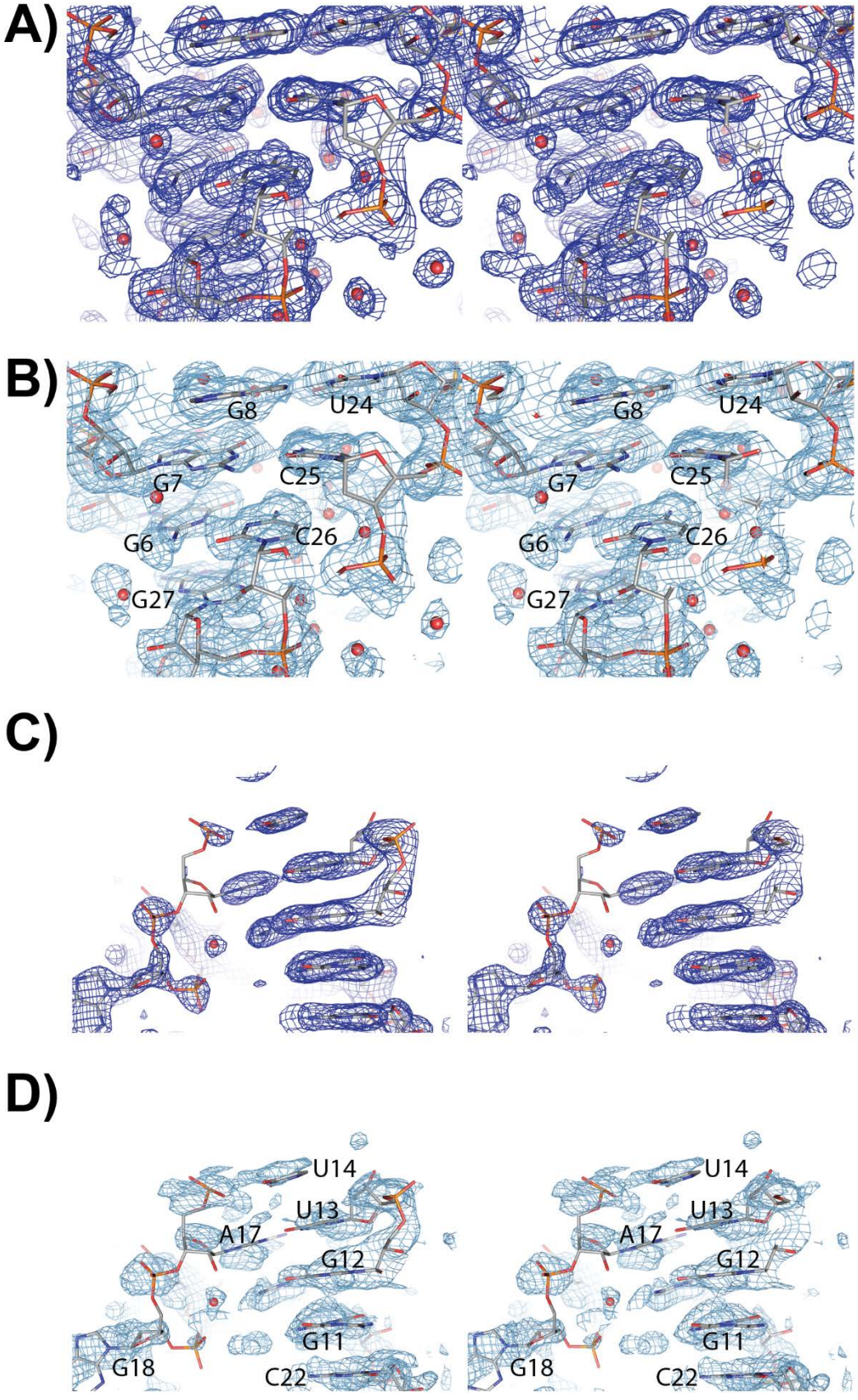
A)
B)
G8
U24
G7
C25
G6
C26
G27
G8
U24
G7
C25
G6
C26
G27
C)
D)
U14
U13
A17
G12
G11
G18
C22
U14
U13
A17
G12
G11
G18
C22

Supplementary Figure S8. Electron density maps of the *E. coli* tRNA^{Asp}-AS/TSL short unit cell structure. Stereo diagrams showing **2mF$_o$-DF$_c$** (**A** and **C**) and simulated annealing omit maps (**B** and **D**) around different regions of the structure. The maps in panels **A** and **B** show a well-ordered region in the stem, whereas panels **C** and **D** show the loop region.

REFERENCES

Briand C, Poterszman A, Eiler S, Webster G, Thierry J, Moras D. 2000. An intermediate step in the recognition of tRNA(Asp) by aspartyl-tRNA synthetase. *J Mol Biol* **299**: 1051-1060. doi:10.1006/jmbi.2000.3819

Goldgur Y, Mosyak L, Reshetnikova L, Ankilova V, Lavrik O, Khodyreva S, Safro M. 1997. The crystal structure of phenylalanyl-tRNA synthetase from thermus thermophilus complexed with cognate tRNAPhe. *Structure* **5**: 59-68. doi:10.1016/s0969-2126(97)00166-4

Jenner LB, Demeshkina N, Yusupova G, Yusupov M. 2010. Structural aspects of messenger RNA reading frame maintenance by the ribosome. *Nat Struct Mol Biol* **17**: 555-560. doi:10.1038/nsmb.1790

Reiter NJ, Osterman A, Torres-Larios A, Swinger KK, Pan T, Mondragon A. 2010. Structure of a bacterial ribonuclease P holoenzyme in complex with tRNA. *Nature* **468**: 784-789. doi:10.1038/nature09516

Ruff M, Krishnaswamy S, Boeglin M, Poterszman A, Mitschler A, Podjarny A, Rees B, Thierry JC, Moras D. 1991. Class II aminoacyl transfer RNA synthetases: crystal structure of yeast aspartyl-tRNA synthetase complexed with tRNA(Asp). *Science* **252**: 1682-1689. doi:10.1126/science.2047877

Schmeing TM, Voorhees RM, Kelley AC, Gao YG, Murphy FVt, Weir JR, Ramakrishnan V. 2009. The crystal structure of the ribosome bound to EF-Tu and aminoacyl-tRNA. *Science* **326**: 688-694. doi:10.1126/science.1179700

Seif E, Hallberg BM. 2009. RNA-protein mutually induced fit: structure of Escherichia coli isopentenyl-tRNA transferase in complex with tRNA(Phe). *J Biol Chem* **284**: 6600-6604. doi:10.1074/jbc.C800235200

Shi H, Moore PB. 2000. The crystal structure of yeast phenylalanine tRNA at 1.93 A resolution: a classic structure revisited. *RNA* **6**: 1091-1105. doi:10.1017/s1355838200000364

Tourigny DS, Fernandez IS, Kelley AC, Ramakrishnan V. 2013. Elongation factor G bound to the ribosome in an intermediate state of translocation. *Science* **340**: 1235490. doi:10.1126/science.1235490

Voorhees RM, Weixlbaumer A, Loakes D, Kelley AC, Ramakrishnan V. 2009. Insights into substrate stabilization from snapshots of the peptidyl transferase center of the intact 70S ribosome. *Nat Struct Mol Biol* **16**: 528-533. doi:10.1038/nsmb.1577